

# Design and demonstration of compact, wide bandwidth coupled-resonator filters on a silicon-on-insulator platform

Qing Li, Mohammad Soltani, Siva Yegnanarayanan and Ali Adibi

School of Electrical and Computer Engineering, Georgia Institute of Technology, 777 Atlantic Drive NW, Atlanta, GA 30332-0250  
[qli6@gatech.edu](mailto:qli6@gatech.edu)

**Abstract:** We design and fabricate a compact third-order coupled-resonator filter on the silicon-on-insulator platform with focused application for on-chip optical interconnects. The filter shows a large flat bandwidth (3dB 3.3nm), large FSR (~18nm), more than 18dB out-of-band rejection at the drop port and more than 12 dB extinction at the through port, as well as a negligible drop loss (<0.5dB) within a footprint of 0.0004 mm<sup>2</sup>.

©2009 Optical Society of America

OCIS codes: (130.3120) Integrated optics devices; (230.5750) Resonators

---

## References and links

1. A. Shacham, K. Bergman, and L.P. Carloni, "Photonic Networks-on-Chip for Future Generations of Chip Multi-Processors," *IEEE Trans. Comput.* **57**, 1246-1260 (2008).
2. Y. Vlasov, W. M. J. Green, and F. Xia, "High-throughput silicon nanophotonic wavelength-insensitive switch for on-chip optical networks," *Nature Photon.* **2**, 242 – 246 (2008).
3. F. Xia, M. Rooks, L. Sekaric, and Y. Vlasov, "Ultra-compact high order ring resonator filters using submicron silicon photonic wires for on-chip optical interconnects," *Opt. Express* **15**, 11934-11941 (2007).
4. D. Xu, A. Densmore, P. Waldron, J. Lapointe, E. Post, A. Delage, S. Janz, P. Cheben, J. H. Schmid, and B. Lamontagne, "High bandwidth SOI photonic wire ring resonators using MMI couplers," *Opt. Express* **15**, 3149-3155 (2007).
5. M. A. Popovic, C. Manolatou, and M. R. Watts, "Coupling-induced resonance frequency shifts in coupled dielectric multi-cavity filters," *Opt. Express* **14**, 1208-1222 (2006).
6. Q. Li, S. Yegnanarayanan, A. Atabaki, and A. Adibi, "Calculation and Correction of Coupling-Induced Resonance Frequency Shifts in Traveling-Wave Dielectric Resonators," in *Integrated Photonics and Nanophotonics Research and Applications*, (Optical Society of America, 2008), paper IWH3, <http://www.opticsinfobase.org/abstract.cfm?URI=IPNRA-2008-IWH3>.
7. J. K. S. Poon, J. Scheuer, S. Mookherjee, G. T. Paloczi, Y. Huang, and A. Yariv, "Matrix analysis of microring coupled-resonator optical waveguides," *Opt. Express* **12**, 90-103 (2004).
8. B. E. Little, S. T. Chu, H. A. Haus, J. Foresi, and J.-P. Laine, "Microring resonator channel dropping filters," *J. Lightwave Technol.* **15**, 998-1005 (1997).
9. S. Xiao, M. H. Khan, H. Shen, and M. Qi, "A highly compact third-order silicon microring add-drop filter with a very large free spectral range, a flat passband and a low delay dispersion," *Opt. Express* **15**, 14765-14771 (2007).
10. H. A. Haus, *Waves and fields in optoelectronics* (Prentice-Hall, Englewood Cliffs, NJ, 1984).
11. P. Meystre and M. Sargent III, *Elements of quantum optics*, second edition (Springer-Verlag, Berlin, 1991) Chap.6.
12. B. G. Lee, A. Biberman, P. Dong, M. Lipson, and K. Bergman, "All-Optical Comb Switch for Multiwavelength Message Routing in Silicon Photonic Networks," *IEEE Photon. Technol. Lett.* **20**, 767-769 (2008).
13. B. G. Lee, X. Chen, A. Biberman, X. Liu, I-W. Hsieh, C.-Y. Chou, J. I. Dadap, F. Xia, W. M. J. Green, L. Sekaric, Y. A. Vlasov, R. M. Osgood, Jr., and K. Bergman, "Ultrahigh-Bandwidth Silicon Photonic Nanowire Waveguides for On-Chip Networks," *IEEE Photon. Technol. Lett.* **20**, 398-400 (2008).
14. D. Dimitropoulos, S. Fathpour, and B. Jalali, "Limitations of active free carrier removal in silicon Raman amplifiers and lasers," *Appl. Phys. Lett.* **87**, 261108 1-3(2005).
15. F. Xia, L. Sekaric, and Y. Vlasov, "Mode conversion losses in silicon-on-insulator photonic wire based racetrack resonators," *Opt. Express* **14**, 3872-3886 (2006).

## 1. Introduction

The development of integrated on-chip optical interconnects has inspired a lot of research during the recent years for transporting information between multicore microprocessors [1, 2]. While previous studies have shown that direct replacement of electrical interconnect wiring with optical links is power inefficient, another alternate approach has been proposed, in which an on-chip nanophotonic network is used to switch and route all the available wavelength channels simultaneously to provide the large bandwidth [1, 2]. In this regard, a critical basic element for scalable on-chip optical networks is an optical switch realized using optical filters with a large bandwidth (a few hundred GHz to accommodate large temperature fluctuations and also to support large bandwidth wavelength channels), low crosstalk and negligible insertion loss. Recently, coupled-resonator filters made of planar traveling-wave microresonators have shown promise for this purpose, and such filters have been pursued on silicon-on-insulator (SOI) platform because of its compatibility with CMOS fabrication and potential to achieve integrated ultra-compact structures. In the previous work, a multi-mode interferometer (MMI) scheme has been employed for the coupling between the bus waveguide and the resonator to obtain a large bandwidth [3]. The MMI coupler has the advantages that its coupling strength is less wavelength dependent in addition to being less sensitive to fabrication errors [4]. However, a major drawback of such couplers is the introduction of unavoidable insertion loss at the transition port from/to the waveguide to/from the MMI region, as well as increase in design complexity due to the requirement for extensive numerical computation.

In this paper, we switch to another approach for designing an efficient and large bandwidth filter consisting of coupled racetrack resonators made of single-mode waveguides with the same dimension as the coupling bus waveguide. In this design approach, we benefit from two advantages, namely, 1) the filter design parameters are obtained with less computation effort, and 2) the insertion loss introduced by the coupling between the waveguide and the resonators is negligible. In addition, the coupling-induced resonance frequency shifts (CIFS) is another important issue in coupled-resonators filters. Depending on the resonators geometry and their coupling scheme, CIFS can strongly distort the filter response [5, 6]. We have included this issue in our design and using our compensation techniques we have been able to suppress this effect.

## 2. Filter design and fabrication

Our goal is to design an add-drop flat-band filter with a large bandwidth (3dB bandwidth ~3.3nm) and a large FSR (~18nm) to achieve similar performances as demonstrated in the previous work [2,3]. For the demonstration purpose we focus on the design and demonstration of a 3<sup>rd</sup>-order filter as shown in Fig. 1(a). All the designs, simulations and measurements performed in this paper are for the TE polarization, i.e. electric field is predominantly in the plane of the structure. From the FSR consideration, the perimeter of individual racetrack resonators that constitute the 3<sup>rd</sup>-order filter must be around 31  $\mu\text{m}$ , assuming a group index of 4.22 for a single-mode ridge waveguide with dimension of 500nm wide and 215nm high above the oxide. From the bandwidth and the FSR considered above, the power coupling coefficient  $\kappa^2$  between the resonator and waveguide and the mutual power coupling coefficient  $\kappa_m^2$  between the resonators (see Fig. 1(a)) are required to be 0.82 and 0.18, respectively ( $\kappa, \kappa_m$  itself is the field coupling coefficient), which are extracted from the rigorous transfer matrix analysis [7]. Note that for large bandwidth filter design, where stronger coupling between the waveguide and resonators is required, the well-known narrow-band filter synthesis based on the first-order temporal coupled-mode theory (CMT) technique fails to generate accurate design parameters [8] (for example, for 3<sup>rd</sup>-order narrow-band filters, the flat-band condition requires that  $\kappa_m^2/\kappa^2=1/8$  [8, 9], which is different from what we have calculated above). The reason for this discrepancy lies in the fact that in temporal CMT, the resonator field energy is represented by a normalized parameter so that the resonator energy uniformly scales with any change in that parameter [8,10,11]. However, when the resonator is strongly coupled to

another resonator or waveguide, this assumption is no longer valid. In fact, because of the strong perturbation, the energy (power) distribution in the resonator at the coupling region differs from the other parts of the resonator (see the Appendix A). We find that for flat-band filter design, by introducing an equivalent length instead of the resonator perimeter for the end resonators (see Appendix A, Eq. (9)), which are strongly coupled to bus waveguide, the CMT still works quite well (details in Appendix A). Figure 1(b) shows the simulated transmission response at the drop port using the transfer matrix analysis [7]. Also, the ideal 3<sup>rd</sup>-order flat-band (Butterworth) response predicted by the modified CMT is plotted, assuming a coupling quality factor ( $Q$ ) of 470 between the bus waveguide and the first resonator in the filter (Appendix A, Eq. (10)). As shown in Fig. 1(b), good agreement is observed between the two methods in the passband. However, in the out-of-band region, the modified CMT gives a larger out-of-band rejection ratio. The difference is ascribed to the fact that CMT only considers one FSR in the analysis and the contributions from neighboring FSRs are not accounted, which can limit the rejection ratio especially in the small finesse filters.

In the compensation of CIFS, we use the symmetric coupling scheme, as we proposed in [6], which is graphically shown in Fig. 1(a), where the bus waveguide-resonator coupling geometry is symmetric along the wave propagation direction instead of the conventional straight bus waveguide coupling. In this case, the coupling structure is phase-matched and only the second-order coupling effect is present [6].

Based on the filter parameters regarding the FSR and bandwidth and also the compactness of the structure, the following parameters are specified according to the filter requirements and simulations: the bending radius of the resonators is chosen to be  $3\ \mu\text{m}$ , the interaction coupling length  $L$  is found to be  $7\ \mu\text{m}$ , and the four gaps as shown in Fig. 1(a) are found to be [45 nm, 120 nm, 120 nm, 45 nm], respectively [details see Appendix B.]. The CIFS calculation shows that the resonance of the middle resonator is about 200 GHz larger than that of the other two side resonators, where the coupling to the bus waveguide is strong [6]. We accordingly compensate this, by increasing the middle resonator's perimeter by adding a length  $D$  as shown in Fig. 1(a) to be 14 nm.

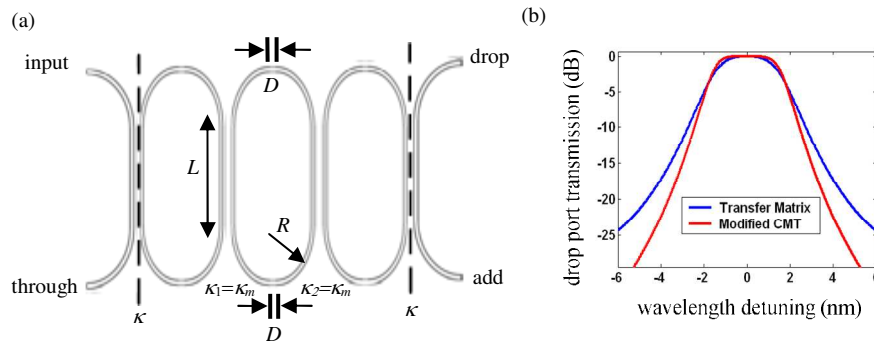


Fig. 1. (a) Schematic of a 3<sup>rd</sup>-order filter made of three racetrack resonators; the length of the center resonator is adjustable, as shown by the length parameter  $D$ , to compensate the CIFS effect; the two vertical dash lines are the symmetry axis of the waveguide-resonator coupling structure, as proposed in the symmetric-coupling scheme [6] (b) drop port transmission response of the 3<sup>rd</sup>-order filter given by transfer matrix analysis and the modified CMT, respectively.

The filter is fabricated on a SOI wafer with 215nm lightly p-doped silicon on top of a  $1\ \mu\text{m}$  buried oxide layer. The device is patterned using a dilute hydrogen silsesquioxane (HSQ) negative electron resist with a thickness of 110 nm in a JBX-9300FS electron beam lithography (EBL) system. After developing the pattern, it is etched in an inductively-coupled plasma etching system with a  $\text{Cl}_2$  chemistry. Figure 2 shows scanning-electron micrographs (SEM) of the fabricated device. The characterization of the filter is performed by coupling light from a modulated tunable laser to the input facet of the waveguide through a tapered lens

fiber. The output signal is collected at the output facet by another tapered lens fiber and sent to the detector and subsequently to a lock-in amplifier for signal detection and noise filtering.

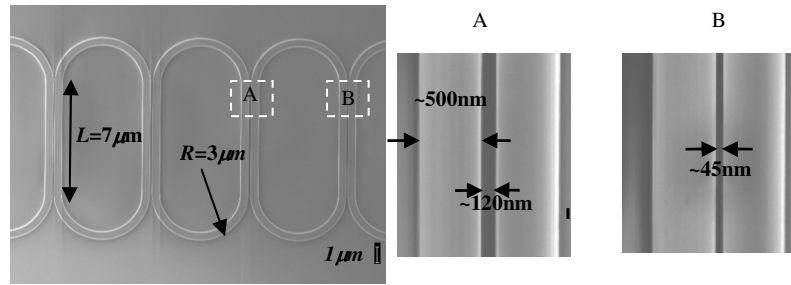


Fig. 2. Scanning-electron micrographs of the fabricated 3<sup>rd</sup>-order filter made of three coupled racetrack resonators. Each individual resonator is made of a waveguide with a 500 nm width and a 215 nm height and an outer bending radius of 3  $\mu\text{m}$ . The figures at the right show a portion of the coupling regions with the gaps as specified.

### 3. Experimental results and discussion

Figure 3(a) shows the measured TE-polarized transmission spectrum of the filter shown in Fig. 2. The data shows that our filter has a 3-dB bandwidth of about 3.3 nm and a FSR of about 18 nm. The out-of-band rejection is more than 18 dB at the drop port, and the crosstalk is less than -12 dB at the through port. The small fluctuation seen in Fig. 3 is mainly from the remaining Fabry-Perot effect, which arises from reflections at the waveguide/air interface at the cleaved facets. Note that the Fabry-Perot effect is partially removed by the lock-in amplifier, where the detected signal is averaged over a certain wavelength range ( $\sim 30$  pm in our measurement) during signal integration. To evaluate the performance of the individual resonators that constitute the filter, a single resonator coupled to a waveguide is fabricated on the same chip. The measured intrinsic  $Q$  is found to be between 30,000~40,000. Such a relatively high intrinsic  $Q$  gives a theoretical drop loss of less than 0.5 dB for the 3<sup>rd</sup>-order filter made of such resonators with the filter parameters given in Section 2. From Fig. 3(a) we can see that the peak drop response is even a little bit higher than the through one, which is due to the alignment error. The actual insertion loss is then inferred from measurement of Fabry-Perot effect without the lock-in amplifier, since the depth of Fabry-Perot variation is determined by the propagation loss. By comparing Fabry-Perot response at the drop and through port, we find the measured insertion loss agree quite well with the theoretical prediction, that is, less than 0.5 dB.

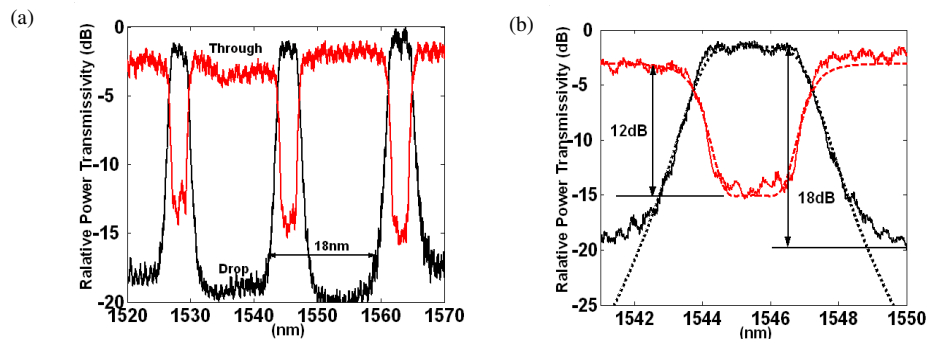


Fig. 3. (a) Experimental responses of the drop and through ports of the 3<sup>rd</sup>-order filter shown in Fig. 2(a); (b) Experimental (solid) and simulated (dashed) responses of the filter around 1550 nm showing one FSR.

The experimental data is also compared with the simulation results over one FSR, as shown in Fig. 3(b). The limited extinction (12 dB) of the through port is because of the

deviation of the mutual power coupling coefficients, i.e.  $\kappa_1^2$  and  $\kappa_2^2$  as shown in Fig. 1(a), from the designed value  $\kappa_m^2$ . This deviation is caused by the fabrication errors which are on the order of 5-10 nm in the EBL step and the subsequent developing step. By fitting the experimental data with temporal CMT simulation, we are able to extract the actual mutual power coupling coefficients ( $\kappa_1^2=0.9 \kappa_m^2$  and  $\kappa_2^2=1.1 \kappa_m^2$ ). Moreover, the almost symmetric response of the through port indicates that the CIFS is largely compensated by our CIFS compensation technique. The out-of-band rejection at the drop port is limited to 18 dB while the designed value is more than 25dB (see Fig. 1(a)). We ascribe this to the sensitivity of our setup and also the observed strong light scattering from the shallow 1  $\mu\text{m}$  buried oxide layer. We expect to obtain an improvement in the out-of-band rejection by increasing the thickness of the buried oxide layer.

To employ such a coupled-resonator filter device for an on-chip data transport with large data rate capacity, we anticipate each passband of the demonstrated filter (where three of them are shown in Fig. 3(a)) to be used for a single wavelength channel, and all the wavelength channels are deflection routed simultaneously by aligning them to each FSR of the filter [2,12,13]. Moreover, due to the challenge with thermal drift between the on-chip switch and the off-chip laser sources, it becomes necessary to add thermal guard bands for +/- 15° C temperature drifts [2], which is already implemented in our filter device. To realize filters suitable for wideband interconnects, the key challenges include: 1) optimization of FSR of the filter to the desired level and 2) mode engineering of the waveguide to achieve single mode operation and low group-delay skew across the entire wavelength range. The switching function based on this optical filter can be achieved by tuning the middle resonator out of its resonance through free carrier injection [2]. Because of the low group-delay of the filter (less than 2 ps), the switching speed is mainly determined by the free carrier dynamics. The large bandwidth of the filter requires a large amount of free carrier injections, which will possibly limit the switching speed [14], and further investigations such as novel implementation of p-n junction and introduction of fast recombination centers in the silicon waveguide to reduce the free carrier lifetime are needed.

#### 4. Conclusion

We have demonstrated a compact and on-chip 3<sup>rd</sup>-order filter made of three coupled racetrack resonators on a SOI platform. We obtain a very flat-band filter response by applying a CIFS compensation technique to the filter structure, as well as through good fabrication control. The individual resonators that constitute the filter show a relatively large intrinsic  $Q$  (~40,000) with a good repeatability of fabrication. The resulting 3<sup>rd</sup>-order filter has a large bandwidth (~3.3 nm), a large FSR (~18 nm), a very low insertion loss (<0.5dB), and a small footprint of about 0.0004 mm<sup>2</sup>, which enables it as a key building block component for on-chip optical networks.

#### Appendix A. Field nonuniformity inside a strongly coupled resonator and the modified CMT

As mentioned, in the temporal CMT, it is customary to represent the resonator field energy with a normalized parameter, which is a function of time but not of space, so that the resonator energy uniformly scales with any change in that parameter [10]. The essence of this assumption is that in high- $Q$  resonator, the mode amplitudes and phases are fairly uniform throughout the resonator [11]. However, when the resonator is strongly coupled to another resonator or waveguide, this assumption is no longer valid. In fact, because of strong perturbation, the energy (power) distribution in the resonator at the coupling region strongly differs from the other parts of the resonator. To see this, we consider the simplest case in which a resonator is coupled to a waveguide as shown in Fig. 4(a). In this figure, we assume that  $s_1$  and  $s_2$  are the fields at two arbitrary points inside the resonator at the two sides far from the coupling region. They are normalized in a way that  $|s_1|^2$  and  $|s_2|^2$  stand for the powers at the specified points inside the resonator. Also,  $s_i$  and  $s_r$  are the normalized fields at the input and

output ports in the waveguide with their powers given by  $|s_i|^2$  and  $|s_l|^2$ , respectively. The coupling interaction between the resonator and the waveguide can be described by the following matrix [10],

$$\begin{bmatrix} s_2 \\ s_l \end{bmatrix} = \begin{bmatrix} \sqrt{1-\kappa^2} & i\kappa \\ i\kappa & \sqrt{1-\kappa^2} \end{bmatrix} \begin{bmatrix} s_1 \\ s_i \end{bmatrix} \quad (1)$$

where  $\kappa^2$  is the power coupling coefficient between the resonator and the waveguide. In writing Eq. (1), we have not included the phase propagation term from  $s_l$  to  $s_2$  (we adopt the  $\exp(i(kz-\omega t))$  format). Instead, we include this part in the phase propagation from  $s_2$  to  $s_l$ , which turns out to be,

$$s_1 = s_2 \exp(i\beta L) \quad (2)$$

where  $\beta$  is the waveguide propagation constant and  $L$  is the perimeter of the resonator. In Eq. (2) we have assumed that the intrinsic  $Q$  of the resonator is high enough so that the propagation loss is negligible. Combining Eqs. (1) and (2), we have

$$s_1 = \frac{i\kappa}{\exp(-i\beta L) - \sqrt{1-\kappa^2}} s_i \quad (3)$$

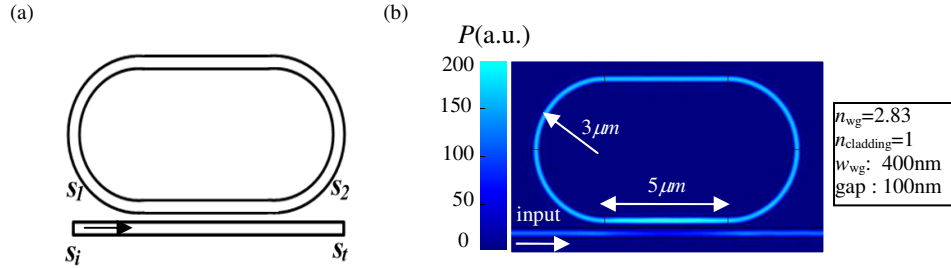


Fig. 4. (a) Schematic of a resonator coupled to a waveguide; (b) power distribution inside the resonator with a strong coupling to the bus waveguide, where a source is implemented. The simulation details are provided in the right box: the waveguide (WG) width is 400nm; the refractive indices of the waveguide and cladding are 2.83 and 1, respectively. The bending radius of the resonator is  $3 \mu\text{m}$ ; the straight coupling length is  $5 \mu\text{m}$  and the gap between the resonator and waveguide is 100nm. In this simulation the polarization is TE (magnetic field is normal to the plane of the paper) and the racetrack resonance wavelength is 1572nm.

By expanding the propagation constant  $\beta(\omega)$  around the resonator resonance frequency ( $\omega_0$ ) as  $\beta \approx \beta_0 + (\Delta\omega)/v_g$  ( $\Delta\omega = \omega - \omega_0$  and  $v_g$  is the group velocity at the resonance frequency), we have

$$s_1 \approx \frac{i\kappa}{(1-\sqrt{1-\kappa^2}) - i\frac{L}{v_g}\Delta\omega} s_i \quad (4)$$

In the meantime, the CMT gives [8, 10]

$$\frac{da}{dt} = -(i\omega_0 + \frac{1}{\tau})a + i\mu s_i \quad (5)$$

where  $a$  is the normalized field amplitude (with  $|a|^2$  represents the total energy inside the resonator);  $\tau$  is the amplitude decay time-constant,  $\mu$  is the mutual coupling between the waveguide and the resonator and is related to  $\tau$  from power conservation:  $\mu^2 = 2/\tau$  [8,10]. By solving Eq. (5) in the frequency domain, we have

$$a = \frac{i\mu}{\frac{1}{\tau} - i\Delta\omega} s_i \quad (6)$$

Comparing Eq. (4) and Eq. (6), we find a resemblance in these expressions. However, in Eq. (4)  $|s_1|^2$  represents the power at a point inside the resonator while  $|a|^2$  in Eq. (6) represents the total energy inside the resonator. To do the conversion between power and energy, we use the relationship

$$Power = \frac{Energy}{T} = \frac{|a|^2 v_g}{L} \quad (7)$$

where  $T$  is the total traveling time inside the resonator. However, the power calculated in Eq. (7) is the average power. It is not equal to  $|s_1|^2$ , which is specified as the power far from the coupling region. As an example, Fig. 4(b) shows the 2-dimensional numerical simulation result for the power (energy) distribution inside a strongly coupled resonator. Figure 4(b) clearly shows that the power at the coupling region is larger than that of the places which are far from the coupling region (this is valid when the power coupling coefficient increases monotonically along the coupling region). Therefore, the average power is larger than  $|s_1|^2$ . Based on this field nonuniformity, we have to introduce an equivalent perimeter  $L'$  for  $|s_1|^2$  to do power-energy conversion,

$$|a|^2 = Power \frac{L}{v_g} = |s_1|^2 \frac{L'}{v_g} (L' > L) \quad (8)$$

Combing Eq. (4), (6), (8) together, and make the identification of each corresponding term, we finally arrive at

$$L' = \frac{2}{1 + \sqrt{1 - \kappa^2}} L \quad (9)$$

$$\mu^2 = 2 \frac{v_g}{L} (1 - \sqrt{1 - \kappa^2})$$

In the weak coupling case (i.e.  $\kappa^2 \ll 1$ ), expanding Eq. (9) to the first order, we find that  $L'$  reduces to the resonator perimeter  $L$  and  $\mu^2$  is equal to  $\frac{v_g}{L} \kappa^2$ , which is the expression used in the narrow-band filter synthesis technique [8].

We know that for flat-band coupled-resonator devices, only the end resonators (i.e. the first and the last one that are coupled to the bus waveguides) have strong coupling, and the mutual power coupling between adjacent resonators are small [8]. Thus, it is a fairly good approximation to consider the field nonuniformity only for the end resonators. Therefore, the coupling  $Q$  of the end resonator is given by

$$Q = \frac{\pi n_g L}{\lambda(1 - \sqrt{1 - \kappa^2})} \quad (10)$$

and the total coupling  $Q$  of the whole structure is half of the value given by Eq. (10). By doing this modification, the CMT still works well and the design parameters can be generated accordingly with the same procedures as shown in the narrow-band filter synthesis technique [8].

## Appendix B. Physical implementation of the design parameters

The dimension of the waveguide we are using is 500nm wide and 215nm high above the buried oxide. We choose the bending radius of the resonator to be  $3\mu m$  as a balance between the compactness and the radiation loss consideration. The power coupling coefficients, as extracted from the transfer matrix or the modified CMT as given in appendix A, is 0.82 for  $\kappa^2$  and 0.18 for  $\kappa_m^2$ . For the parallel waveguide directional coupler, the power coupling coefficient is given by [10]

$$\kappa_p^2 = \sin^2(\Delta\beta_1 z) \quad (11)$$

where  $\Delta\beta_1$  is the first-order coupling parameter given by  $\Delta\beta_1 = (\beta_s - \beta_{as})/2$  ( $\beta_s$  and  $\beta_{as}$  are the propagation constants for the symmetric and anti-symmetric supermodes of the directional coupler respectively);  $z$  is the effective coupling length, and is given by  $z = L + Z_0$ . Here  $L$  is the straight coupling length of the racetrack resonator, as shown in Fig. 1(a) and  $Z_0$  is the effective coupling length contributed by the bending part, which is approximated to be  $1\mu m$  for the bending radius we choose. Since the desired FSR requires the total resonator perimeter to be around  $31\mu m$ , we choose  $L$  to be  $7\mu m$ , so  $z = 8\mu m$ . Knowing the power coupling coefficients, based on Eq. (11), the gaps can be chosen from three dimensional mode solver for the parallel waveguide coupler to achieve the desired  $\Delta\beta_1$ . As a result, we find the first gap between the resonator and waveguide to be 45nm. Through numerical simulation, we find even at such a small gap, the mode-conversion loss is negligible [15], and it is safe to work in this small gap region though it poses more challenges to the fabrication accuracy control.

As for the CIFS compensation, we choose to adjust the resonator perimeter instead of other methods such as changing the cross section of the ring resonator [9]. This is because the effective refractive index of the mode is very sensitive to the change of the waveguide cross section. For example, we have to increase about 28nm length of the middle resonator to compensate the CIFS for the filter demonstrated in this paper, while for the same amount of CIFS we only need to increase its waveguide width by less than 5nm, which is difficult to accurately achieve considering the random fabrication errors on the same order.

## Acknowledgments

This work was supported by Air Force Office of Scientific Research under Contract No. FA9550-06-01-2003 (G. Pomrenke).